An alternative to the traveling-wave approach for use in two-port descriptions of acoustics bores

Eric Ducasse

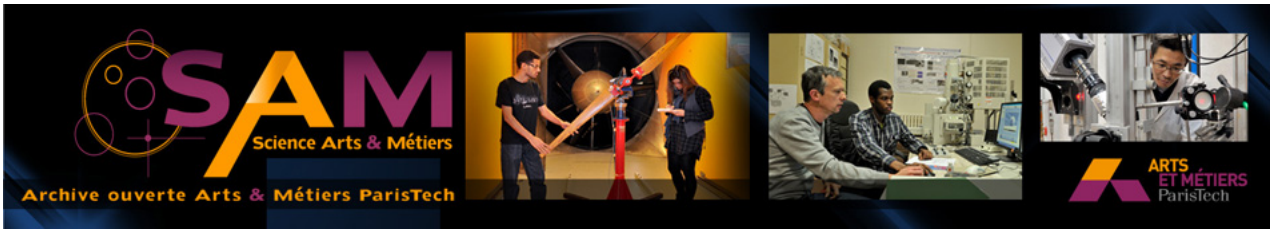

An alternative to the traveling-wave approach for use in two-port descriptions of acoustic bores

Éric Ducasse
École Nationale Supérieure d'Arts et Métiers, C.E.R. de Bordeaux-Talence, 33405 Talence cedex, France
eric.ducasse@ensam.eu
(Abbreviated title: Two-port description of acoustic bores)

ABSTRACT

For more than a decade, the digital waveguide model for musical instruments has been improved through the simulation of cylindrical and conical bores. But several difficulties remain, such as instabilities due to growing exponentials which appear when two conical bores are connected with decreasing taper. In this paper, an alternative overcoming these difficulties is proposed and can be extended to shapes other than cylinders, cones, and hyperbolic horns. A two-port model with more general state variables than usual traveling waves works efficiently for any shape without discontinuities in cross-section. The equations for connecting separate elements at discontinuities make this two-port model appropriate for use in time domain simulation of the physical behavior of the wind instrument and its interactions with the player. The potential of this new approach is illustrated by several detailed examples.

PACS numbers: 43.75.Ef, 43.60.Gk

1 Introduction

Two decades ago, sound synthesis by physical modeling of musical instruments, was at an embryonic stage[1,2], though already raising high expectations. Since the end of the eighties[3,4], this method of sound synthesis has improved steadily, computers have become faster and faster, and nowadays, commercial products based on this technology are available. In 1996, Smith[5] summed up the situation in this domain of research and pointed out several difficulties. To create a physical model of a wind instrument, a suitable model of a bore with varying cross section needs to be implemented. In this context, previous descriptions of wind instruments are briefly reviewed, separated into two groups.

The first approach considers a wind instrument to be composed of a non-linear excitation mechanism - the mouthpiece - and of a resonator - the body - which is a linear element. The resonator is completely characterized by either its reflection function or its input impedance[6–12]. This *lumped* approach, which gives precise results and a good match between experiments and theory for a given note, has a disadvantage: the properties of the resonator are fixed. Thus, simulations close to real playing situations, including realistic transients between several notes, are difficult to obtain. For instance, the dynamic closing of tone-holes by fingers or keys, or the motion of a trombone slide, are not simulated.

For sound synthesis, the relationship between the player and the instrument needs to be taken into account[4,13–17], including the actions of lips, tongue, blown air, and fingers. A *distributed* approach is generally used. Because modularity is a key to this second approach – a wind instrument is composed of a mouthpiece, tubes, tone-holes, a slide, a bell, ...etc –, a tube has to be modeled as an element which can be connected at both ends to other elements. In this approach, piecewise element modeling techniques are generally employed for acoustic bores with varying cross-section. Each element is a two-port which can be seen as a *waveguide* provided it is either a cylinder, a truncated cone, or a hyperbolic horn. It has been shown that in a cylindrical bore, the acoustical pressure wave is the sum of two traveling plane waves which propagate in opposite directions; the same holds for a conical bore with two traveling spherical waves[6,8]. Further, previous works show[18] that in cylindrical and hyperbolic bores, *"flow waves propagate without dispersion"*. Thus, "*A convenient model of a waveguide* [can

also be built] *using piecewise hyperbolic elements*"[18]. In the context of a step by step calculation in discrete time domain, this approach gives the *digital waveguide*[4] model which is used by almost all the authors[4,13–23] . This method is efficient due to its very low computational load.

The digital waveguide model was first conceived for a cylindrical bore without losses[4]. It has been progressively improved by the addition of fractional delays[24,23,25], visco-thermal losses, and conical bores[13–23]. Nevertheless, difficulties are encountered as soon as the bore is non-cylindrical[9]. The connecting equations with separate elements are indeed rather complicated, showing integral terms that may generate growing exponentials, for instance in the case of two conical bores connected with "*a decreasing taper*"[10]. From another point of view[18], these instability phenomena correspond to the existence of "*trapped modes*" in addition to normal "*traveling modes*".

In this paper, Section II summarizes the traveling-wave approach and points out the sources of instabilities in models using piecewise element techniques for waveguides. Section III presents a new stable two-port which is usable not only for cylinders, truncated cones, and hyperbolic horns but also for tubes of arbitrarily varying cross-section. Finally, detailed examples illustrating the potential of this model are given in Section IV.

2 *Instabilities in waveguide modeling*

2.1 Traveling signals in lossless bores

2.1.1 Pressure waves in cylindrical and conical bores

In a bore with varying cross-section, a commonly used model for lossless propagation is based on the following equation, usually named the "*Horn Equation*"[26–30]:

$$\frac{\partial^2 p}{\partial x^2} - \frac{1}{c^2}\frac{\partial^2 p}{\partial t^2} = \frac{-S'(x)}{S(x)}\frac{\partial p}{\partial x} \tag{1}$$

where p is the mean acoustic pressure in a cross-section S of the bore, depending on abscissa x and time t, and c the sound speed (usually $340\,\mathrm{m}\cdot\mathrm{s}^{-1}$). It is assumed that the wave fronts are planar and that the bore is relatively wide.

After the transformation $p(x,t) = [S(x)]^{-1/2}\ \psi(x,t)$, Eq. (1) becomes:

$$\frac{\partial^2 \psi}{\partial x^2} - \frac{1}{c^2}\frac{\partial^2 \psi}{\partial t^2} = \frac{1}{\sqrt{S(x)}}\frac{\partial^2 \sqrt{S(x)}}{\partial x^2}\psi \tag{2}$$

When the second term of Eq. (2) is zero, mainly in the case of either a cylinder or a truncated cone, Eq. (2) becomes the standard wave equation, the solution of which is the sum of two traveling waves, giving:

$$p(x,t) = \frac{\psi^+(x - c\,t)}{\sqrt{S(x)}} + \frac{\psi^-(x + c\,t)}{\sqrt{S(x)}} \tag{3}$$

Using a common approximation for the Euler equation, where u is the acoustic volume velocity through cross-section $S(x)$, and ρ_0 the air mean density (usually $1.21\,\mathrm{kg}\cdot\mathrm{m}^{-3}$):

$$\rho_0 \frac{\partial u}{\partial t} + S(x)\frac{\partial p}{\partial x} = 0 \tag{4}$$

Equations (3) and (4) now give the volume velocity u:

$$u(x,t) = \frac{S(x)}{\rho_0\, c}\left[\frac{\psi^+(x - c\,t) - \psi^-(x + c\,t)}{\sqrt{S(x)}} + \frac{c\,S'(x)}{2\,S(x)}\int_{-\infty}^{t} p(x,\sigma)\,d\sigma\right] \tag{5}$$

2.1.2 Volume velocity waves in cylindrical and hyperbolic bores

Similarly, a "*Horn Equation for volume velocity*" can be given[18, Eq.(3.126)] :

$$\frac{\partial^2 u}{\partial x^2} - \frac{1}{c^2}\frac{\partial^2 u}{\partial t^2} = \frac{S'(x)}{S(x)}\frac{\partial u}{\partial x} \tag{6}$$

After the transformation $u(x,t) = \sqrt{S(x)}\,\phi(x,t)$, Eq. (6) becomes[18, Eq.(3.137)]:

$$\frac{\partial^2 \phi}{\partial x^2} - \frac{1}{c^2}\frac{\partial^2 \phi}{\partial t^2} = \sqrt{S(x)}\,\frac{\partial^2 \left[S(x)^{-1/2}\right]}{\partial x^2}\,\phi \tag{7}$$

In the case of either a cylinder or a hyperbolic horn, the solution of Eq. (7) is the sum of two traveling waves which gives:

$$u(x,t) = \sqrt{S(x)}\,\phi^+(x - c\,t) + \sqrt{S(x)}\,\phi^-(x + c\,t) \tag{8}$$

The mass conservation law being:

$$S(x)\frac{\partial p}{\partial t} + c^2\rho_0\frac{\partial u}{\partial x} = 0 \tag{9}$$

The acoustic pressure can be deduced:

$$p(x,t) = \frac{\rho_0\,c}{S(x)}\left(\sqrt{S(x)}\,(\phi^+(x - c\,t) - \phi^-(x + c\,t)) - \frac{c\,S'(x)}{2\,S(x)}\int_{-\infty}^{t} u(x,\sigma)\,d\sigma\right) \tag{10}$$

A numerical model using digital waveguides in conjunction with a decomposition into a pair of traveling waves is deduced from Eqs. (3) and (5) when the air column is cylindrical or conical, or from Eqs. (8) and (10) when the air column is hyperbolic.

2.2 Description of the waveguide model

Consider both ends ($x = 0$ and $x = L$) of a conical bore. Substituting $q^+(x,t)$ and $q^-(x,t)$ for $\left[S(x)^{-1/2}\right]\,\psi^+(x - c\,t)$ and $\left[S(x)^{-1/2}\right]\,\psi^-(x + c\,t)$, respectively, Eqs. (3) and (5) become:

$$\begin{aligned}
q^+(L,t) &= \frac{1}{\zeta}\,q^+(0,t-\tau)\\
q^-(0,t) &= \zeta\,q^-(L,t-\tau)\\
p(0,t) &= q^+(0,t) + q^-(0,t)\\
u(0,t) &= \frac{S(0)}{\rho_0\,c}\left[q^+(0,t) - q^-(0,t) + \frac{c\,S'(0)}{2\,S(0)}\int_{-\infty}^{t} p(0,\sigma)\,d\sigma\right]\\
p(L,t) &= q^+(L,t) + q^-(L,t)\\
u(L,t) &= \frac{S(L)}{\rho_0\,c}\left[q^+(L,t) - q^-(L,t) + \frac{c\,S'(L)}{2\,S(L)}\int_{-\infty}^{t} p(L,\sigma)\,d\sigma\right]
\end{aligned} \tag{11}$$

where L is the length of the tube, $\tau = L/c$ the propagation delay between the extremities, and $\zeta = [S(L)/S(0)]^{1/2}$ the radii ratio.

The first two equations of System (11) define a waveguide filter including a double delay line and radius correctors[31]. These equations constitute the uniform transmission-line and transformer components of Fig. 1. Visco-thermal losses can be lumped in additional filters. The transfer function of these filters is $G(s) = \exp\left(-\beta\,L\sqrt{s}/r\right)$ for cylindrical tubes[32,33,20], where s is the complex variable of the Laplace transformation, $r = \sqrt{S/\pi}$ the radius, $\beta = \left[\sqrt{l_v} + (\gamma - 1)\sqrt{l_t}\right]/\sqrt{c}$ (usually $1.6 \times 10^{-5}\,\mathrm{s}^{1/2}$) a constant representing the visco-thermal effects, γ the ratio of specific heats, l_v and l_t the characteristic lengths of the viscous and thermal effects[e.g. 7,34,35,33,11]. It can be extended to truncated cones by taking r as an equivalent radius (*e.g.*[14] $r = (r_L - r_0)\,[\log(r_L/r_0)]^{-1}$ where r_0 and r_L are the radii at the two ends).

The integral terms[36,14] in System (11) explain the instabilities encountered in the case of conical bores, as detailed in the following section.

Similarly, a waveguide model of a hyperbolic bore can be defined by substituting $q^+(x,t)$ and $q^-(x,t)$ respectively for $\sqrt{S(x)}\,\phi^+(x - c\,t)$ and $\sqrt{S(x)}\,\phi^-(x + c\,t)$. Integral terms appear in this case also.

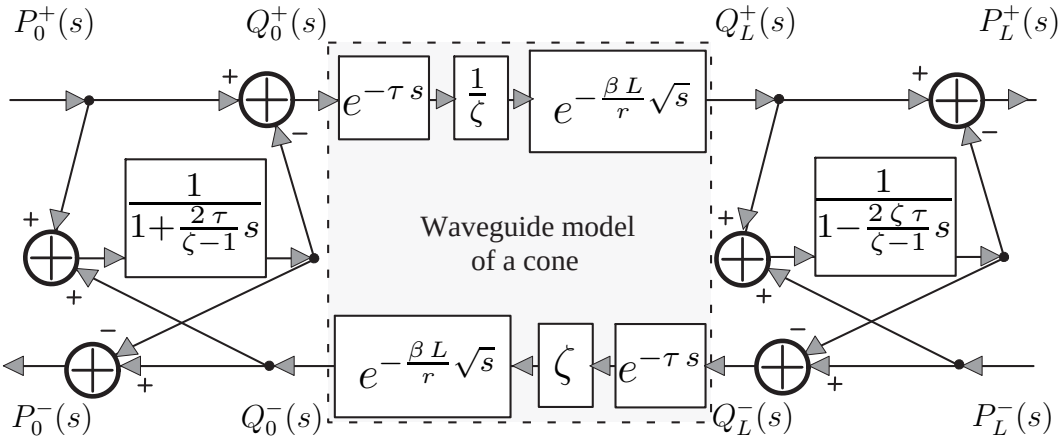

Figure 1: Block-diagram of a conical bore where both the usual waveguide state variables q^+, q^- and the new state variables p^+, p^- can be observed.

2.3 Instabilities in a junction of two conical tubes

The instability phenomena associated with conical bores have been demonstrated through various approaches[5,10,21,18] In the case of two conical tubes connected with a continuous radius (*cf.* Fig. 2), continuity of mean pressure, conservation of volume velocity, and System (11) give after a Laplace transform:

$$\begin{aligned} &Q^+_{left}(s) + Q^-_{left}(s) = Q^+_{right}(s) + Q^-_{right}(s) = P_J(s) \\ &Q^+_{left}(s) - Q^-_{left}(s) + \frac{c\, r'_{left}}{r_J\, s} P(s) = Q^+_{right}(s) - Q^-_{right}(s) + \frac{c\, r'_{right}}{r_J\, s} P_J(s) \end{aligned} \tag{12}$$

where $p_J(t)$ is the mean pressure at the junction, r' the taper (derivative of r with respect to x), and the following convention is adopted: if w is a signal or a vector of signals, $W = \mathcal{L}(w)$ is its Laplace transform defined for all s by $W(s) = \int_{-\infty}^{+\infty} w(t)\, e^{-st}\, dt$. The other quantities are defined in Fig. 2.

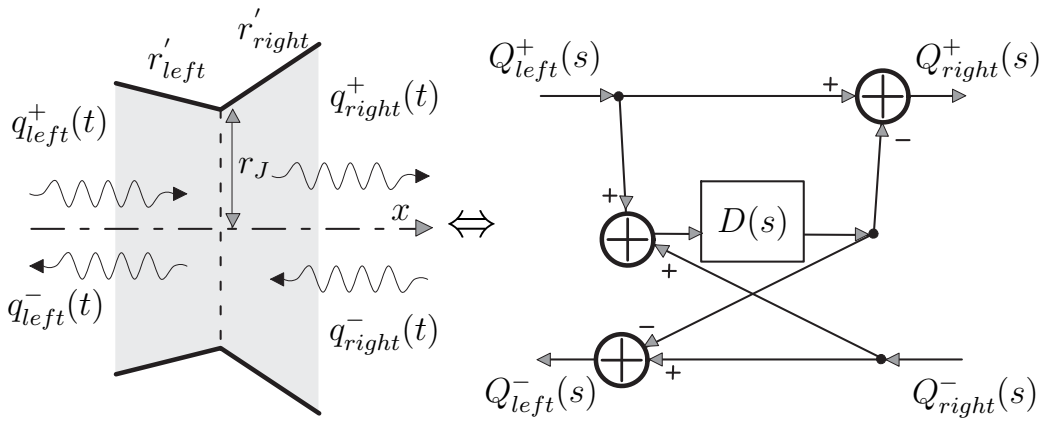

Figure 2: A junction of two conical tubes with radius continuity and its block-diagram.
$D(s) = \left\{1 + 2\, r_J\, s / \left[c\, \left(r'_{right} - r'_{left}\right)\right]\right\}^{-1}$ is the transmittance of a first-order filter which is unstable provided $r'_{right} < r'_{left}$.

If the taper is not continuous, Eq. (12) becomes:

$$\begin{aligned} Q^-_{left}(s) &= Q^-_{right}(s) - \left[1 + \frac{2\,r_J}{c\,(r'_{right} - r'_{left})}\,s\right]^{-1} \left[Q^+_{left}(s) + Q^-_{right}(s)\right] \\ Q^+_{right}(s) &= Q^+_{left}(s) - \left[1 + \frac{2\,r_J}{c\,(r'_{right} - r'_{left})}\,s\right]^{-1} \left[Q^+_{left}(s) + Q^-_{right}(s)\right] \end{aligned} \tag{13}$$

This equation (13) can be translated into the block-diagram of Fig. 2, containing a first-order filter[21]. This filter is stable for increasing taper ($r'_{right} > r'_{left}$) and unstable for decreasing taper ($r'_{right} < r'_{left}$), as shown in previous work[10]. Even if visco-thermal losses are introduced, instabilities remain.

The next section presents an alternative to the usual traveling-waves approach. This approach suppresses instabilities.

3 A two-port with physically obtainable traveling waves as inputs and outputs

In this approach, traveling waves are not formulated inside the modeled bore. Instead they are formulated outside it, in cylinders which are connected to it so that the cross section is continuous (see Fig. 3a). This lumped approach has already been used in the "*reflection function*" characterization of a resonator given by Schumacher[1]: when a cylinder with an anechoic termination at one end is connected to the input of the resonator with continuity of cross-section, the reflection function corresponds to a reflected traveling wave which is the response of the resonator to an incoming impulse wave. This approach differs from the usual piecewise element modeling techniques. It has been already mentioned in Scavone[23] (pp. 119-123 and Fig. 3.25) to solve an example problem of instability. Since incoming and outgoing waves are physically obtainable in cylinders, with anechoic terminations at unconnected ends in this case, the modeled bore is necessary seen as a passive two-port (see Fig. 3b) without any stability problem. It should be noticed that, in the "*traveling and trapped modes*" approach (Berners[18], Section 3.1.3), trapped modes disappear as soon as the bore has cylindrical terminations at both ends.

3.1 Hypotheses

The following hypotheses are made[11]: the bore section is quasi-circular; its area $S(x)$ which is not too small[33] ($\alpha = \beta\,c/(2\sqrt{S}\sqrt{f}) \ll 1$, where f is the frequency) or too large, is a continuous function with moderate variations ($S'(x)$ is defined almost everywhere and bounded). The tube is also quasi-rectilinear or has only very smooth bends. Subject to these conditions we can adopt the plane wave approximation: the acoustic pressure p and velocity v are considered uniform over the section $S(x)$ as well as functions of abscissa x and time t. This is in fact the mean over the bore, (*cf.* Fig. 3a) obtained by integration over the boundary layer.

3.2 Equations

The following system is adopted in accordance with Polack[11, Eq.(41)]: the first equation is the mass conservation law where ρ is the acoustic density, the second one is an extended approximation of the Euler equation and the last one is the equation of state for the air.

$$\begin{aligned} &S(x)\frac{\partial \rho}{\partial t} + \rho_0 \frac{\partial u}{\partial x} = 0 \\ &\rho_0 \frac{\partial u}{\partial t} + 2\,\rho_0\,c\,\sqrt{\frac{\pi}{S(x)}}\,\beta\,\frac{\partial^{\frac{1}{2}} u}{\partial t^{\frac{1}{2}}} + S(x)\frac{\partial p}{\partial x} = 0 \\ &p = c^2 \rho \end{aligned} \tag{14}$$

Two state variables are chosen to determine a numerical solution in the discrete time-domain. These state variables may differ from the ones used in traveling-wave approaches.

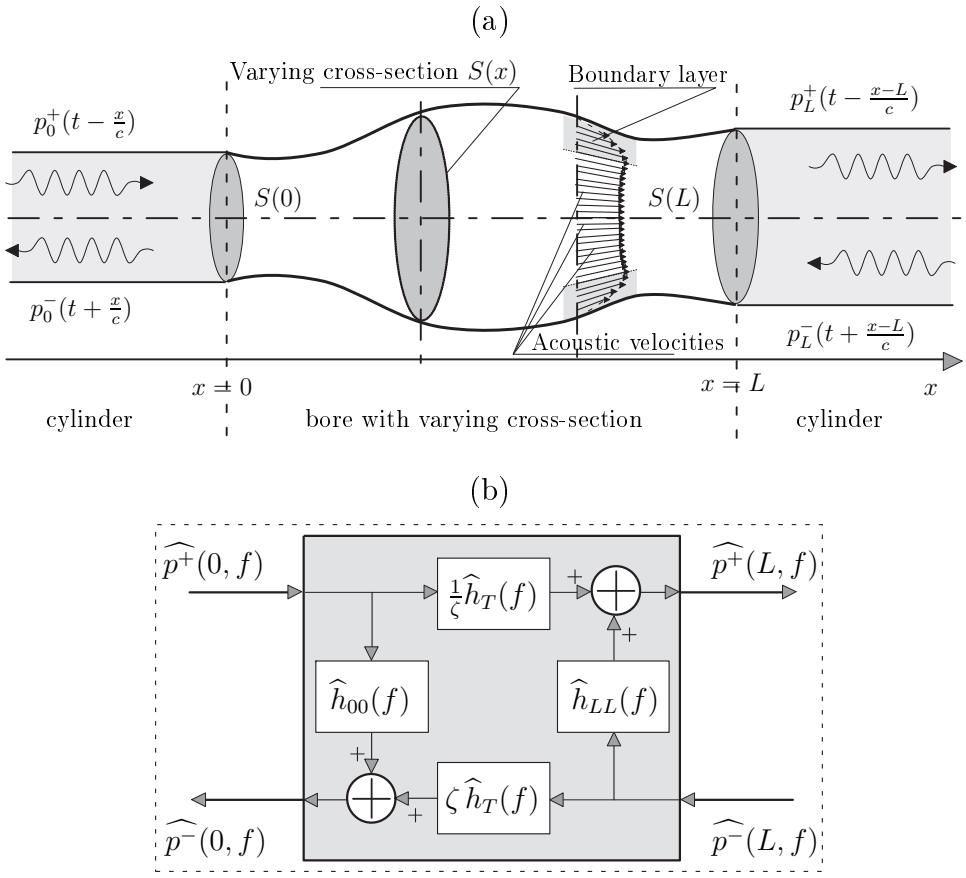

Figure 3: (a) A bore with varying cross section. Both extremities of this bore are connected to cylinders without cross-section discontinuities. Each cylinder has an anechoic termination at its unconnected end. p_0^+, p_0^-, p_L^+ and p_L^- are traveling waves. The typical boundary layer in the air column is shown with the acoustic velocity distribution. (b) Block-diagram of a two-port modeling the air column inside the main bore, with the inputs $p^+(0,t)=p_0^+(t)$ and $p^-(L,t)=p_L^-(t)$, and the outputs $p^-(0,t)=p_0^-(t)$ and $p^+(L,t)=p_L^+(t)$.

3.3 Choosing the suitable state variables

The choice of state variables, including input and output signals, is fundamental to a convenient description of a physical phenomenon. The following example shows how the effect of such a choice can explain phenomena like non-causality or growing exponentials, as pointed out in previous studies[9,18,37,38]. Suitable state variables are then given for a bore with varying cross-section.

3.3.1 Preliminary

Let a physical system be described by the following differential equation:

$$\begin{aligned}&\frac{d\,w(t)}{dt}-500\,w(t)=\frac{d\,v(t)}{dt}+1500\,v(t)\\&\text{for all } t<0,\ v(t)=0,\ w(t)=0\end{aligned}\tag{15}$$

Its input and output can *a priori* supposedly be chosen freely.

If v and w are respectively selected as input and output, the system is unstable because its impulse response h_1 contains a growing exponential:

$$h_1(t)=\delta(t)+2000\,\epsilon(t)\,e^{+500t}\tag{16}$$

where δ is the Dirac impulse pseudo-function[39] and ϵ the Heaviside step function.

On the contrary, if w is the input and v the output, the system is stable because its impulse response is:

$$h_2(t)=\delta(t)-2000\,\epsilon(t)\,e^{-1500t}\tag{17}$$

It is also possible to take the input as $s_{in} = w + v$ and the output as $s_{out} = w - v$. Equation (15) becomes:

$$\begin{aligned} &\frac{d\,s_{out}(t)}{dt} + 500\,s_{out}(t) = 1000\,s_{in}(t) \\ &\text{for all } t < 0,\ s_{in}(t) = 0,\ s_{out}(t) = 0 \end{aligned} \tag{18}$$

In this third case, the physical phenomenon is modeled as a stable first-order system and its impulse response contains neither growing exponentials nor pseudo-functions. It can be noticed that in any case for a given input e_{in} and a given output s_1 and for any number a, the output modification $s_2(t) = s_1(t) + a\,e_{in}(t)$ changes neither the stability nor the characteristic time of the model.

This example emphasizes that stability is not intrinsic to a given physical phenomenon but notably depends on the choice of the input, which has to be physically obtainable. Pseudo-functions can generally be eliminated in the impulse response by modifying the output.

3.3.2 From the reflection function to a two-port model

The reflection function[1] h_r of a woodwind resonator verifies $p_0^- = h_r \star p_0^+$ where p_0^+ and p_0^- are traveling pressure waves in a lossless cylinder connected to the entrance of the resonator, with continuity of cross-section (*cf.* the left half of Fig. 3a), and the operator $\star$ is the convolution (for all t, $(h_r \star p_0^+)(t) = \int_{-\infty}^{+\infty} h_r(t-\xi)\,p_0^+(\xi)\,d\xi$). The reflection function is necessarily stable for physical reasons (the resonator is a passive system and the input is physically obtainable) and can be considered as causal if the following hypothesis is laid down: we can neglect the thickness ε of the air slice between $x = -\varepsilon$ and $x = 0$ (in the cylinder, just before the entrance of the resonator) which is directly influenced by the resonator shape.

Following this idea, the state vector $P = \binom{p^+}{p^-}$ is chosen to describe the acoustic state of the air column, the signals p^+ and p^- being defined as follows:

$$\begin{aligned} p^+(x,t) &= \frac{1}{2}\left[p(x,t) + \frac{\rho_0 c}{S(x)}\,u(x,t)\right] \\ p^-(x,t) &= \frac{1}{2}\left[p(x,t) - \frac{\rho_0 c}{S(x)}\,u(x,t)\right] \end{aligned} \tag{19}$$

$$\begin{aligned} p(x,t) &= p^+(x,t) + p^-(x,t) \\ u(x,t) &= \frac{S(x)}{\rho_0 c}\left[p^+(x,t) - p^-(x,t)\right] \end{aligned} \tag{20}$$

These signals are traveling waves only in the model of a cylindrical bore without losses, *i.e.* $p^+(x,t)$ can be written $p^+(x-ct)$ and $p^-(x,t)$, $p^-(x+ct)$. In any other case, p^+ and p^- are not traveling on the whole air column but can be qualified as "*locally-traveling*" (in a slice of air of area S and infinitesimal thickness). The connecting equations of the bore with any other element of the instrument remain elementary (continuity of mean pressure and flow conservation) because of Eq. (20), similar to the last four equations of System (11) but without any integral term. Above all, the main advantage is that any piece of bore with a varying cross section can be modeled as a single two-port (*cf.* Fig. 3b), which is necessarily stable and causal for reasons similar to the reflection function case (*cf.* Fig. 3a).

After a Fourier transform, Systems (14) and (20) give the following non-linear differential system:

$$\frac{\partial}{\partial x}\widehat{P}(x,f) = A\left[S(x), S'(x), f\right]\,\widehat{P}(x,f) \tag{21}$$

where $\widehat{P}(x,f)$ is the Fourier transform of the state vector P at the frequency f:

$$\widehat{P}(x,f) = \begin{bmatrix} \widehat{p^+}(x,f) \\ \widehat{p^-}(x,f) \end{bmatrix} = \begin{bmatrix} \displaystyle\int_{-\infty}^{+\infty} p^+(x,t)\,e^{-2i\pi f t}\,dt \\ \displaystyle\int_{-\infty}^{+\infty} p^-(x,t)\,e^{-2i\pi f t}\,dt \end{bmatrix} \tag{22}$$

and

$$A(S,S',f)=\begin{bmatrix} \dfrac{-2\,i\,\pi\,f}{c}-\dfrac{(1+i)\,\beta\,\pi\,\sqrt{f}}{\sqrt{S}}-\dfrac{S'}{2S} & \dfrac{(1+i)\,\beta\,\pi\,\sqrt{f}}{\sqrt{S}}+\dfrac{S'}{2S} \\ \dfrac{-(1+i)\,\beta\,\pi\,\sqrt{f}}{\sqrt{S}}+\dfrac{S'}{2S} & \dfrac{2\,i\,\pi\,f}{c}+\dfrac{(1+i)\,\beta\,\pi\,\sqrt{f}}{\sqrt{S}}-\dfrac{S'}{2S} \end{bmatrix} \tag{23}$$

Systems like Eq. (21) are generally solved by numerical techniques. The transfer matrix $T(f)=\begin{bmatrix} T_{11} & T_{12} \\ T_{21} & T_{22} \end{bmatrix}$ of the locally-traveling waves, from the end at $x=0$ to that at $x=L$, verifies $\widehat{P}(L,f)=T(f)\,\widehat{P}(0,f)$ and can be deduced from Eqs. (21) to (23).

The scattering matrix $H(f)$ verifying $\begin{bmatrix} \widehat{p^-}(0,f) \\ \widehat{p^+}(L,f) \end{bmatrix}=H(f)\begin{bmatrix} \widehat{p^+}(0,f) \\ \widehat{p^-}(L,f) \end{bmatrix}$ is then deduced from the transfer matrix:

$$H(f)=\begin{bmatrix} \widehat{h}_{00}(f) & \widehat{h}_{L0}(f) \\ \widehat{h}_{0L}(f) & \widehat{h}_{LL}(f) \end{bmatrix}=\frac{1}{T_{22}}\begin{bmatrix} -T_{21} & 1 \\ T_{11}T_{22}-T_{12}T_{21} & T_{12} \end{bmatrix} \tag{24}$$

where h_{jk} is the impulse response from the end at $x=j$ to the end at $x=k$, $\widehat{h}_{jk}$ its Fourier transform, and H_{jk} its Laplace transform.

In the scattering matrix, reciprocity implies the existence of a single transfer function $\widehat{h}_T(f)$:

$$\widehat{h}_T(f)=\zeta\,\widehat{h}_{0L}(f)=\frac{1}{\zeta}\,\widehat{h}_{L0}(f) \tag{25}$$

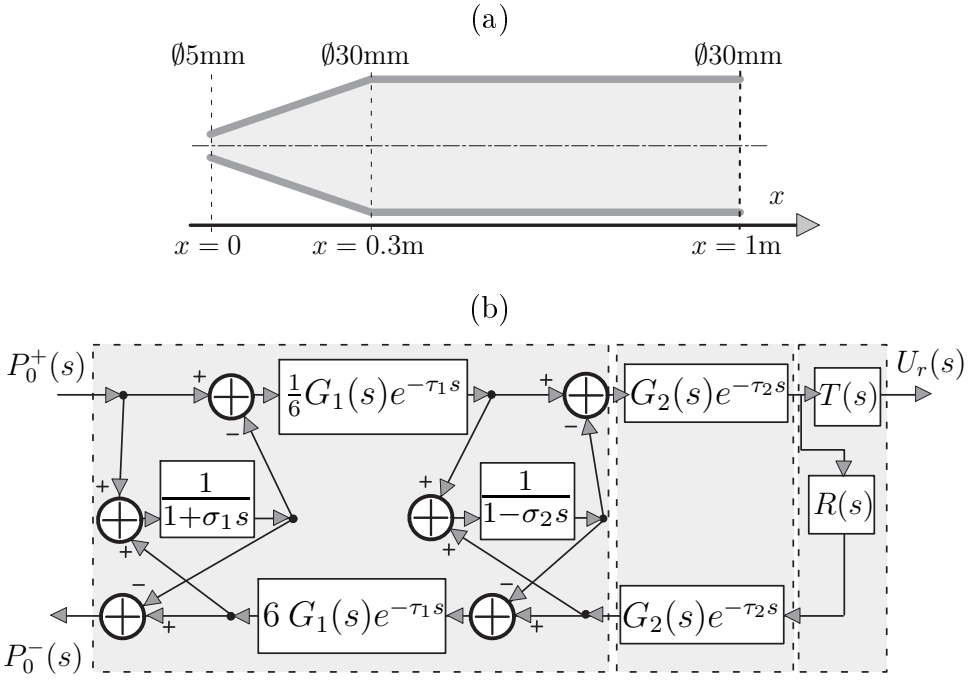

Figure 4: (a) A bore built with a truncated cone and a cylinder (from Agulló *et al.*[9], Fig. 10, p.1611) and (b) its block-diagram including the bell radiation.

It has to be noticed that, in all simulated cases (*cf. e.g.* Fig. 5), the four transmittances in the scattering matrix correspond to causal stable filters with fast-decreasing impulse responses, contrary to other methods[9,37,38]. Accordingly, the present method is promising for time-domain simulations, all the more so as usual techniques of transfer matrix calculation[7] can be used for complex resonators including discontinuities, side-holes or higher modes.

In the case of a conical bore, it can be observed in the next section that these new state variables suppress the instabilities pointed out above.

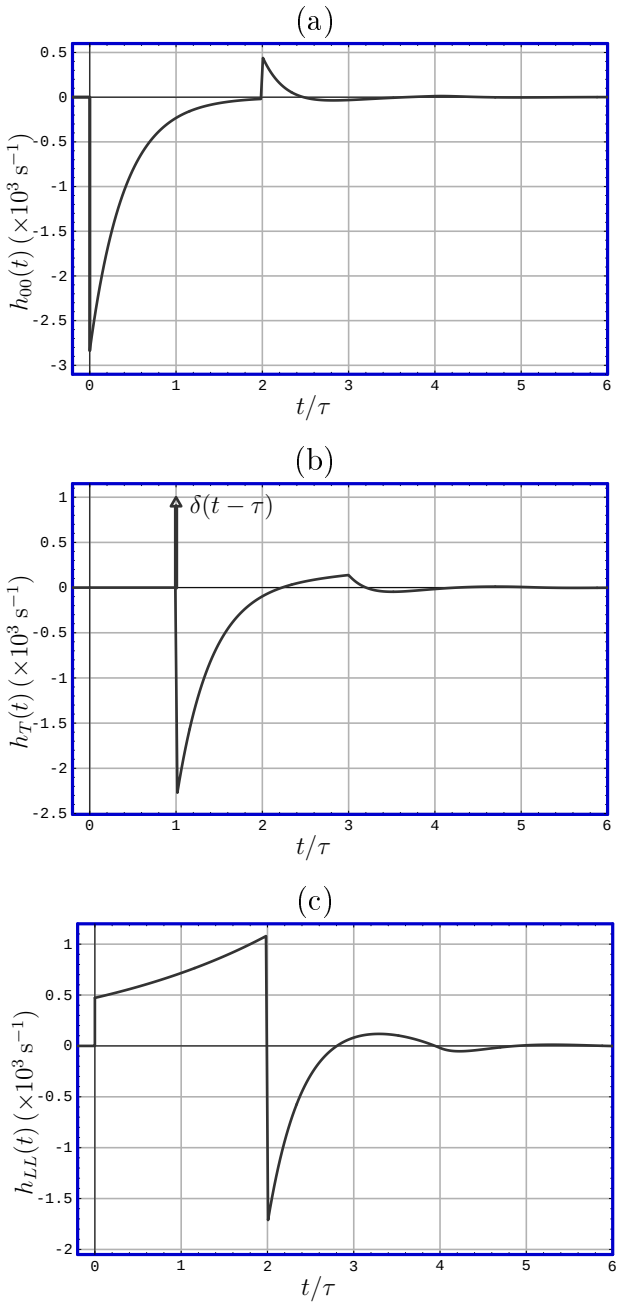

Figure 5: Continuous-time impulse responses (the calculation is made in Section 3.4, Eq. (30)) for the conical part of the bore which is given in Fig. 4. $\tau \approx 0.88\,\mathrm{ms}$ and $\zeta = 6$.

3.4 How instabilities vanish in the waveguide model of a conical bore

The block-diagram of a conical tube in the waveguide approach is only the middle element of the block-diagram drawn on Fig. 1. In the present approach, the whole block-diagram includes junctions with virtual external cylinders at both ends. On the left side $r_J = r_0$, $r'_{left} = 0$, $r'_{right} = (\zeta-1)\,r_0/L$, and $D(s) = [1 + 2\,\tau\,s/(\zeta-1)]^{-1}$. On the right side $r_J = r_L$, $r'_{left} = (\zeta-1)\,r_L/(\zeta\,L)$, $r'_{right} = 0$, and $D(s) = [1 - 2\,\zeta\,\tau\,s/(\zeta-1)]^{-1}$.

The scattering matrix of the conical tube is deduced from Fig. 1:

$$\begin{aligned} H_{00}(s) &= \frac{(\zeta-1)\,[\zeta-1-2\zeta\,\tau s+(2\tau s-\zeta+1)G(s)^2\,e^{-2\tau s}]}{(2\zeta\,\tau s-\zeta+1)\,(2\tau s+\zeta-1)+(\zeta-1)^2G(s)^2\,e^{-2\tau s}} \\ H_T(s) &= \frac{\zeta\,(2\tau s)^2\,G(s)\,e^{-\tau s}}{(2\zeta\,\tau s-\zeta+1)\,(2\tau s+\zeta-1)+(\zeta-1)^2G(s)^2\,e^{-2\tau s}} \\ H_{LL}(s) &= \frac{(\zeta-1)\,[2\tau s+\zeta-1-(2\zeta\,\tau s+\zeta-1)G(s)^2\,e^{-2\tau s}]}{(2\zeta\,\tau s-\zeta+1)\,(2\tau s+\zeta-1)+(\zeta-1)^2G(s)^2\,e^{-2\tau s}} \end{aligned} \tag{26}$$

If losses are ignored (*i.e.* $G(s) = 1$), H_{00}, H_T, and H_{LL} are functions continuous at $s = 0$: $H_{00}(0) = (1-\zeta^2)/(1+\zeta^2)$, $H_T(0) = 2\zeta/(1+\zeta^2)$, and $H_{LL}(0) = (\zeta^2-1)/(1+\zeta^2)$. Each pole $(a + i\,b)/\tau$ ($a \neq 0$ or $b \neq 0$) of H_{00}, H_T, or H_{LL} verifies:

$$(2\zeta a - \zeta + 1 + i\,2\zeta b)\,(2a + \zeta - 1 + i\,2b) + (\zeta-1)^2\,e^{-2(a+i\,b)} = 0 \tag{27}$$

which implies:

$$\frac{sin(2b)}{2b} = e^{2a}\,\left[1 + \frac{4a\zeta}{(\zeta-1)^2}\right] \tag{28}$$

Consequently $a < 0$ and thus H_{00}, H_T, and H_{LL} are transmittances of stable filters. System (26) can be written:

$$\begin{aligned}
H_{00}(s) &= \frac{\zeta-1}{1-\zeta-2\tau s} - 4(\tau s)^2 \sum_{n=1}^{+\infty} \frac{(\zeta-1)^{2n-1}}{(\zeta-1+2\tau s)^{n+1}(\varsigma-1-2\varsigma\,\tau s)^n}\,e^{-2n\,\tau s} \\
H_T(s) &= -4\zeta\,(\tau s)^2 \sum_{n=0}^{+\infty} \frac{(\zeta-1)^{2n}}{(\zeta-1+2\tau s)^{n+1}(\varsigma-1-2\varsigma\,\tau s)^{n+1}}\,e^{-(2n+1)\,\tau s} \\
H_{LL}(s) &= \frac{1-\zeta}{\zeta-1-2\zeta\,\tau s} - 4\zeta^2(\tau s)^2 \sum_{n=1}^{+\infty} \frac{(\zeta-1)^{2n-1}}{(\zeta-1+2\tau s)^{n}(\varsigma-1-2\varsigma\,\tau s)^{n+1}}\,e^{-2n\,\tau s}
\end{aligned} \tag{29}$$

The initial parts of the three causal impulse responses are deduced from Eq. (29) as follows:

$$\begin{aligned}
h_{00}(t) &= \tfrac{1-\zeta}{2\tau}\,\exp\left[\tfrac{1-\zeta}{2\tau}t\right]\,,\ 0 \leqslant t < 2\tau \\
&= \tfrac{\zeta-1}{4e\,\tau(1+\zeta)^2}\left\{2\left[e^{\zeta}(1+\zeta+\zeta^2) - e(1+\zeta)^2\right] - e^{\zeta}(\zeta^2-1)\tfrac{t}{\tau}\right\}\exp\left[\tfrac{1-\zeta}{2\tau}t\right] \\
&\quad + \tfrac{e^{(1-\zeta)/\zeta}(\zeta-1)}{2\tau\zeta(1+\zeta)^2}\,\exp\left[\tfrac{\zeta-1}{2\zeta\tau}t\right]\,,\ 2\tau \leqslant t < 4\tau \\
&\quad \ldots etc. \\
h_T(t) - \delta(t-\tau) &= 0\,,\ 0 \leqslant t < \tau \\
&= \tfrac{e^{(\zeta-1)/2}\zeta\,(1-\zeta)}{2\tau\,(\zeta+1)}\exp\left[\tfrac{1-\zeta}{2\tau}t\right] \\
&\quad + \tfrac{e^{(1-\zeta)/(2\zeta)}(\zeta-1)}{2\tau\,\zeta\,(\zeta+1)}\exp\left[\tfrac{\zeta-1}{2\zeta\tau}t\right]\,,\ \tau \leqslant t < 3\tau \\
&\quad \ldots etc. \\
h_{LL}(t) &= \tfrac{\zeta-1}{2\zeta\tau}\,\exp\left[\tfrac{\zeta-1}{2\zeta\tau}t\right]\,,\ 0 \leqslant t < 2\tau \\
&= \tfrac{1-\zeta}{4e\,\zeta\,\tau(1+\zeta)^2}\left\{2\left[e^{1/\zeta}(1+\zeta+\zeta^2) - e(1+\zeta)^2\right] + e^{1/\zeta}(\zeta^2-1)\tfrac{t}{\tau}\right\}\exp\left[\tfrac{\zeta-1}{2\zeta\tau}t\right] \\
&\quad + \tfrac{e^{\zeta-1}\zeta^2(1-\zeta)}{2\tau(1+\zeta)^2}\exp\left[\tfrac{1-\zeta}{2\tau}t\right]\,,\ 2\tau \leqslant t < 4\tau \\
&\quad \ldots etc.
\end{aligned} \tag{30}$$

A numerical example is given below.

4 Examples

Three cases are chosen to show the potential of this improved two-port model: the first one, taken from Agulló *et al.*[9], produces some instability effects using the traveling-wave approach[5] and includes cylindrical and conical tubes; the textbook case of the exponential horn follows; and finally, a complex profile of a trumpet bore taken from van Walstijn and Smith[17] is treated.

For a non-cylindrical bore, the numerical determination of the transfer matrix at frequencies lying between 0 and $f_s/2$ (f_s is the sampling frequency), is made by the *Fourth-Order Runge-Kutta Algorithm* with an auto-adaptive step[40] applied to Eqs. (21) and (23). This numerical method is computationally rather expensive but calculation has to be performed only once for a given bore. Exact and numerical calculations of the scattering matrix are compared below for both a conical bore and an exponential horn.

Digital filter design methods are numerous and generally pay great attention to the frequency response magnitude but do not take into account the phase which is very important in acoustic looped systems. As written in van Walstijn and Smith[17], "*there is a need for more effective digital filter techniques in this context*". Thus, basic weighted least-squares (WLS) design for *Finite Impulse Response* (FIR) digital filters[41–46] is used in these examples to obtain time domain responses. It is obvious that other efficient methods[17] of digital filter design can be used.

Reflection function calculation is performed entirely in the discrete time-domain, using the Levine and Schwinger formulae[47] to design an FIR digital filter for bell radiation[14] (*cf.* Fig. 4b).

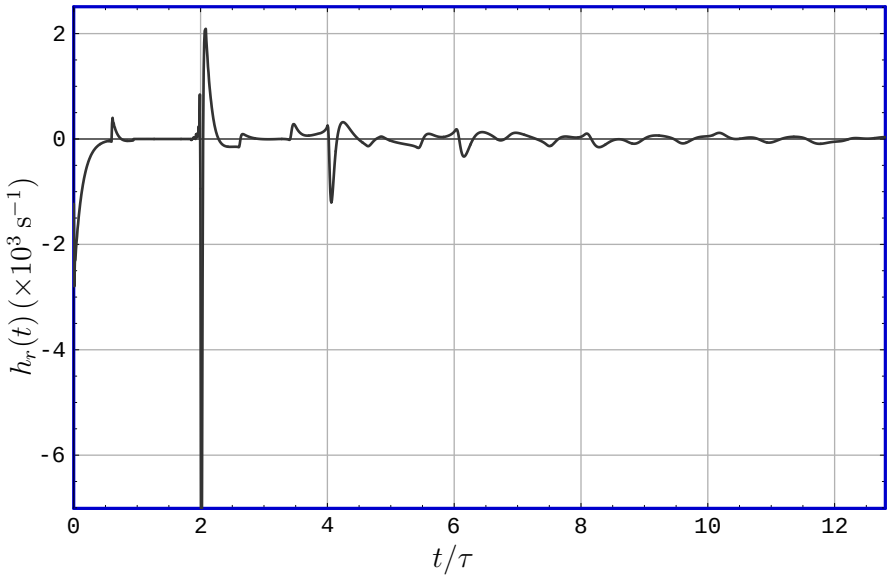

Figure 6: h_r, the reflection function of the bore (*cf.* Fig. 4) at its small end, with a reflection, at the other end, which is calculated by using the Levine and Schwinger formulae[43]. This function is completely calculated in the discrete time-domain with causal digital finite impulse response filters which model the conical part of the bore, the cylindrical one and the radiation. The propagation delay between both ends is $\tau \approx 2.94\,\mathrm{ms}$.

4.1 Discrete time calculation of the reflection function of a cone-cylinder combination

As mentioned in the introduction and shown above in Section 2.3, when several bores are connected with "*decreasing widening rate*"[9] as in Fig. 4 taken from Agulló *et al.*[9] (Fig. 10), stability problems with growing exponentials appear in the usual models. With the improved two-port model, these stability artifacts vanish. The impulse responses h_{00}, h_T, and h_{LL} (*cf.* Eq. (30)) of the conical part of the bore are drawn in Fig. 5. The reflection function of the bore at its small end is drawn in Fig. 6.

Several observations can be made on Fig. 5 about the conical part. For a non-cylindrical bore, it is qualitatively possible to consider, in an air slice of infinitesimal thickness dx, that every traveling wave has an infinitesimal reflection which is proportional to $-dS/S$. At the smaller end, the beginning of the impulse response h_{00} (reflection) is negative and increasing with t because $-dS/S$ is negative and increasing with x. For similar reasons, at the larger end, h_{LL} is positive and increasing between 0 ms and 2τ. Concerning the transmission impulse response after the τ-delayed perfect impulse δ, which is obtained in waveguide models without losses, an additional effect of the taper can be observed after τ. In frequency domain, a good agreement appears on Fig. 7 between the waveguide and numerical techniques. Nevertheless, it seems that the equivalent radius technique[14] in the waveguide approach of conical bores overestimates the visco-thermal losses in both transmission and reflection at the larger end.

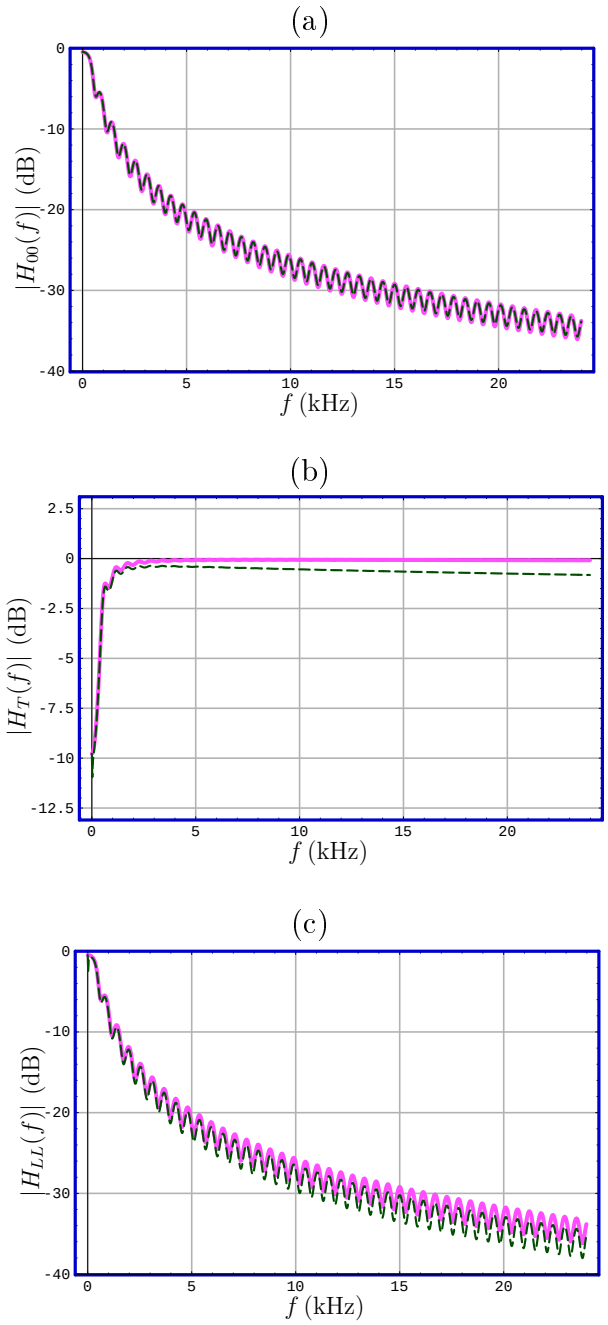

Figure 7: Moduli of transmittance for the conical part of the bore shown in Fig. 4, according to the waveguide approach (*cf.* Section 3.4, Eq. (26), dashed line) and the numerically calculated one from Eqs. (21) and (23) (unbroken line).

4.2 The exponential horn

Let an exponential horn be defined by the radius formulae $r(x) = r_0 \exp(\Lambda x/L)$ where $\Lambda = \log(\zeta)$. In this classical case, Eqs. (21) and (23) admit exact solutions, provided losses terms are neglected, and give the following transmittances in the scattering matrix:

$$
\begin{aligned}
H_{LL}(s) = -H_{00}(s) &= \frac{\Lambda \left[1 - e^{-2\sqrt{(\tau s)^2+\Lambda^2}}\right]}{\sqrt{(\tau s)^2+\Lambda^2}\left[1 + e^{-2\sqrt{(\tau s)^2+\Lambda^2}}\right] + \tau s \left[1 - e^{-2\sqrt{(\tau s)^2+\Lambda^2}}\right]} \\
H_T(s) &= \frac{2\sqrt{(\tau s)^2+\Lambda^2}\, e^{-\sqrt{(\tau s)^2+\Lambda^2}}}{\sqrt{(\tau s)^2+\Lambda^2}\left[1 + e^{-2\sqrt{(\tau s)^2+\Lambda^2}}\right] + \tau s \left[1 - e^{-2\sqrt{(\tau s)^2+\Lambda^2}}\right]}
\end{aligned}
\tag{31}
$$

A comparison between numerical calculation with losses and Eq. (31) is made in Fig. 8 for a horn of 68 cm length, 3 mm and 3 cm radii ($\zeta = 10$ and $\tau = 2$ ms), with a good agreement. The observed cut-off frequency

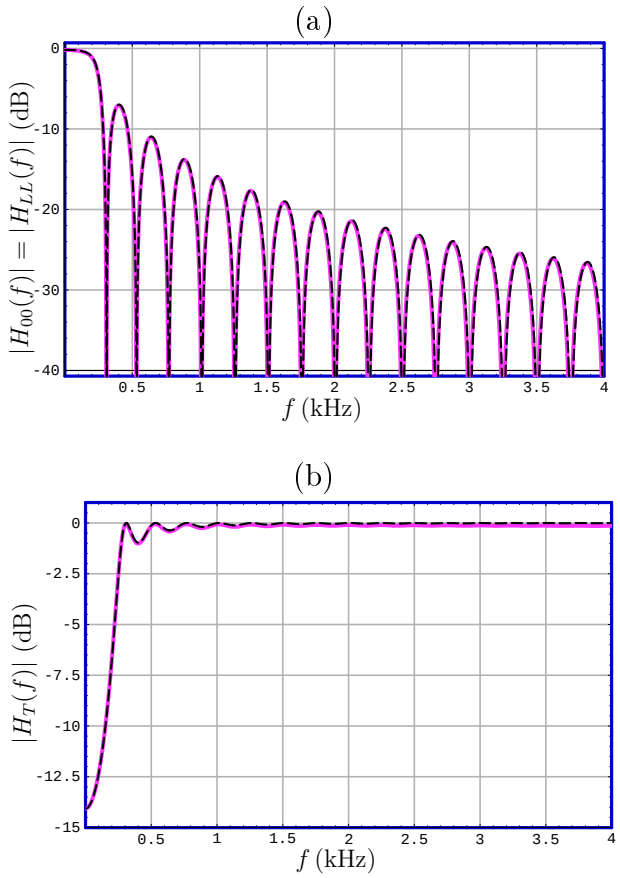

Figure 8: Transmittance modulus of an exponential horn of 68 cm length, 3 mm and 3 cm radii ($\zeta = 10$ and $\tau = 2$ ms). Comparison between exact (without losses, dashed line) and numerical (unbroken line) calculations.

agrees with the expected value $f_c = \Lambda/(2\pi\,\tau) \approx 183.2$ Hz. In the time-domain, the impulse responses can be given using the following property: the function defined for all s by $\left[(\sqrt{s^2+\Lambda^2}-s)/\Lambda\right]^n$ is the Laplace transform of the signal $\mathcal{K}_n$ defined for all t by $\mathcal{K}_n(t) = (n/t)\,\mathrm{J}_n(\Lambda t)\,\epsilon(t)$ provided n is a positive integer, where J_n is the Bessel function of the first kind[48].

After the substitution of:

$$\sum_{n=0}^{+\infty} \frac{(-1)^n \left[\sqrt{(\tau s)^2+\Lambda^2}-\tau s\right]^{2n+1}}{\Lambda^{2n+2}}\, e^{-2n\left[\sqrt{(\tau s)^2+\Lambda^2}-\tau s\right]}\, e^{-2n\tau s} \tag{32}$$

for $\left\{\sqrt{(\tau s)^2+\Lambda^2}\,\left[1+e^{-2\sqrt{(\tau s)^2+\Lambda^2}}\right]+\tau s\,\left[1-e^{-2\sqrt{(\tau s)^2+\Lambda^2}}\right]\right\}^{-1}$, Eq. (31) becomes:

$$\begin{aligned} H_{LL}(s) &= -H_{00}(s) = \frac{1}{\Lambda}(\sqrt{(\tau s)^2+\Lambda^2}-\tau s) + 2\sum_{n=1}^{+\infty}(-1)^n\,\mathcal{B}_{2n}\,e^{-2n\tau s} \\ H_T(s) &= 2\sum_{n=0}^{+\infty}(-1)^n\,\mathcal{B}_{2n+1}\,e^{-(2n+1)\tau s} \end{aligned} \tag{33}$$

where

$$\mathcal{B}_m = \frac{1}{\Lambda^{m+1}}\sum_{k=0}^{+\infty}\frac{(-m)^k}{k\,!}\left\{\Lambda^2\left[\sqrt{(\tau s)^2+\Lambda^2}-\tau s\right]^{m+k-1} - \tau s\,\left[\sqrt{(\tau s)^2+\Lambda^2}-\tau s\right]^{m+k}\right\} \tag{34}$$

After an inverse Laplace transform, Eqs. (33) and (34) give with the convention $\mathcal{K}_0 = 0$:

$$\begin{aligned} h_{LL}(t) &= -h_{00}(t) = \frac{1}{\tau}\,\mathcal{K}_1\left(\frac{t}{\tau}\right) + \frac{2}{\tau}\sum_{n=1}^{+\infty}(-1)^n\, b_{2n}(t-2n\,\tau) \\ h_T(t) &= \delta(t-\tau) + \frac{2}{\tau}\sum_{n=0}^{+\infty}(-1)^n\, b_{2n+1}\,[t-(2n+1)\tau] \end{aligned} \tag{35}$$

where

$$b_m(t) = \sum_{k=0}^{+\infty}\frac{(-m\Lambda)^k}{k\,!}\left[\mathcal{K}_{m+k-1}\left(\frac{t}{\tau}\right) - \frac{1}{\Lambda}\,\mathcal{K}'_{m+k}\left(\frac{t}{\tau}\right)\right] \tag{36}$$

The continuous-time impulse responses are drawn in Fig. 9. They are similar to discrete-time ones which are numerically obtained by inverse discrete Fourier transform.

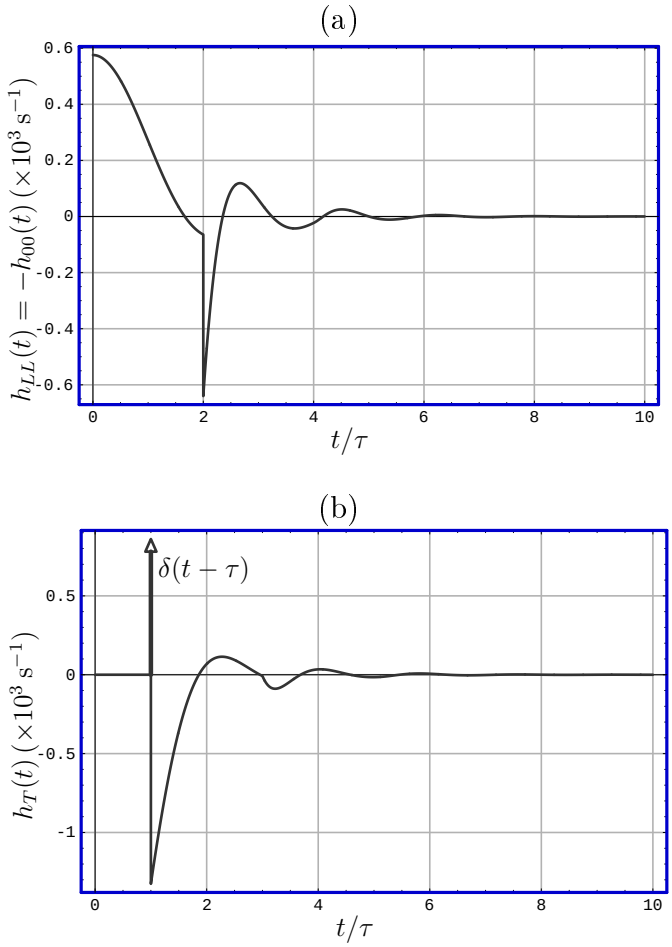

Figure 9: Continuous-time impulse responses of an exponential horn of 68 cm length, 3 mm and 3 cm radii ($\zeta = 10$ and $\tau = 2$ ms).

4.3 A complex bore profile

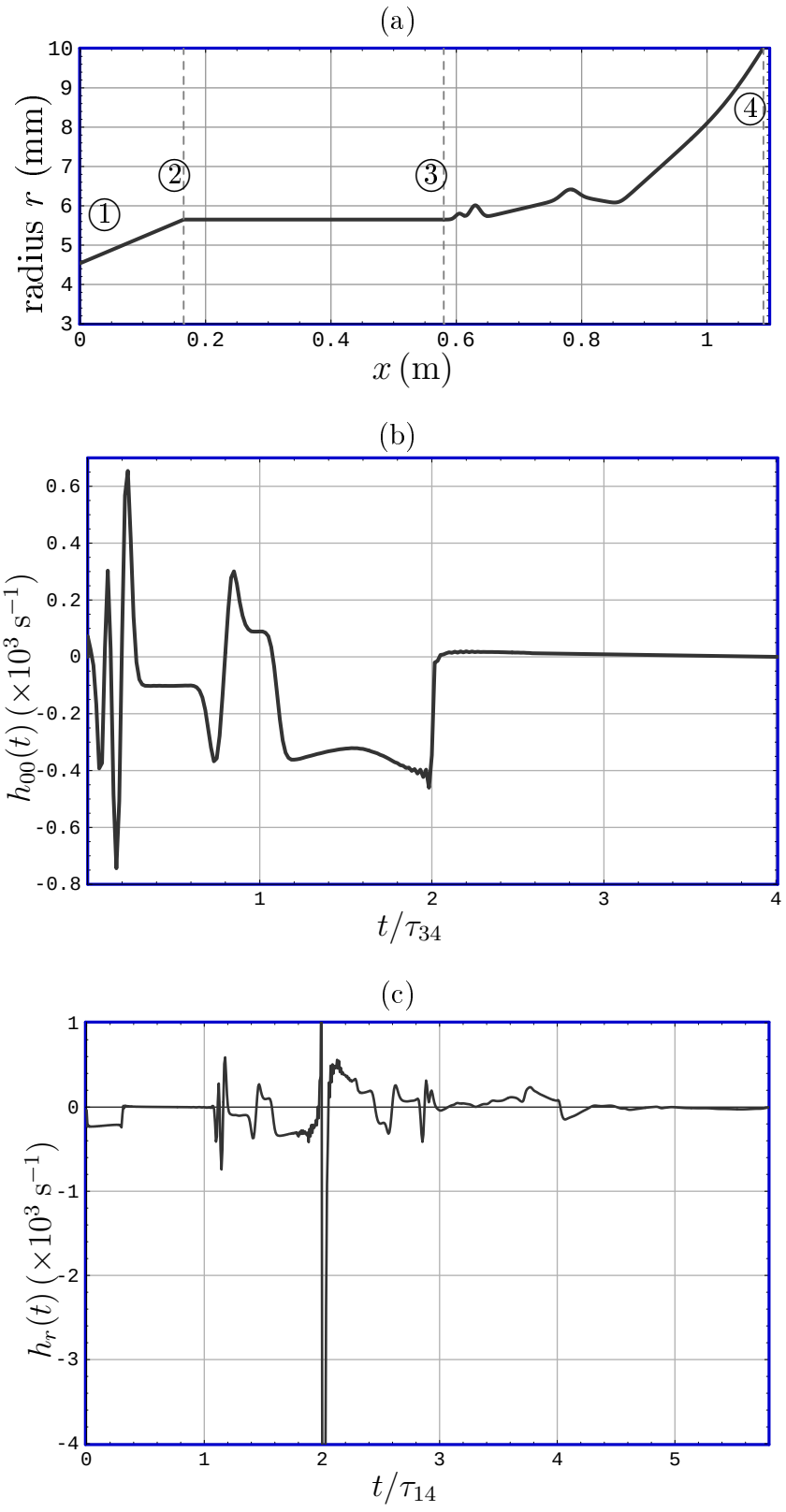

Figure 10: (a) Profile of a trumpet bore (from Fig. 3 in van Walstijn and Smith[17]). The resonator is divided into three parts, from left to right: the "*mouthpipe*" (from ① to ②) is a conical bore of 165 mm length, 4.54 mm and 5.65 mm radii; the "*main bore*" (from ② to ③) is a cylindrical bore, of 415 mm length and 5.65 mm radius; the third part (from ③ to ④) is the beginning, which radius is less than 10 mm, of the "*flared bell*"; the length of this truncated flared bell is 510 mm. (b) Reflection impulse response h_{00} of the flared bell at its small end ③ ($\tau_{34} = 1.5$ ms). (c) Reflection function of the whole trumpet bore at the entrance of the mouthpipe ① ($\tau_{14} \approx 3.2$ ms).

The two-port model can also be used for an arbitrarily varying bore: the profile of a truncated trumpet bore, taken from van Walstijn and Smith[17] (Fig. 3), is given in Fig. 10a. The impulse response h_{00} (reflection) of the truncated flared bell at its small end (mark ③), is given in Fig. 10b. Because "*trajectories*" with a single reflection are predominant, the profile of the bore can almost be followed on the curve of h_{00}, by converting length into time (coefficient $2/c$). The propagation delay between both ends is $\tau_{34} = 1.5\,\mathrm{ms}$. It can be observed that each small profile irregularity produces a significant effect on the h_{00} curve.

The reflection function of the whole truncated trumpet bore at the entrance of the mouthpipe (mark ①) is drawn on Fig. 10c. The total propagation delay between both ends is $\tau_{14} \approx 3.21\,\mathrm{ms}$. Between 0 and $0.3\,\tau_{14}$, the negative reflection inside the mouthpipe (divergent cone) is perceptible. Between $0.3\,\tau_{14}$ and $1.06\,\tau_{14}$, reflections are negligible (cylindrical part). Between $1.06\,\tau_{14}$ and about $2\,\tau_{14}$, the reflection impulse response h_{00} of the truncated flared bell is recognizable. The negative peak, which appears at $2\,\tau_{14}$ and reaches a magnitude of about $1.5 \times 10^4\,\mathrm{s}^{-1}$, results from the reflection at the opening end (mark ④). After about $2\,\tau_{14}$, multiple reflections inside the tube are superimposed, the effects of the three parts of the bore are more difficult to differentiate, even if a kind of $(2\,\tau_{14}, 0)$-centered symmetry can be observed and qualitatively explained by the predominance of trajectories containing three reflections.

5 Concluding remarks

This new two-port model is promising for accurate time-domain simulation of musical wind instruments with an arbitrary bore shape. The present approach based on locally-traveling plane waves may be seen as an alternative to waveguide filter approaches which include piecewise element modeling.

This approach improves time-domain modeling of bores with varying cross section but it is only an element of a complete physical model. This global model could lead to an implementation of a tool for instrument makers, which may enable them to listen to an instrument before it is manufactured. However, improvements are still necessary in the physical modeling of other elements of wind instruments, including their interactions with the player.

Acknowledgments

The author is grateful to Noam Amir, Jean-Pierre Dalmont, Joël Gilbert, and Jean Kergomard for their suggestions and enlightening comments on his work.

References

[1] R. T. Schumacher, "Ab initio calculations of the oscillations of a clarinet," Acustica **48**, 71-85 (1981).

[2] M. E. McIntyre, R. T. Schumacher, and J. Woodhouse, "On the oscillations of musical instruments," J. Acoust. Soc. Am. **74**, 1325-1345 (1983).

[3] J.-M. Adrien, and E. Ducasse, "Dynamic modeling of instruments for sound synthesis," In Proc. Int. Conf. Acoustics, Belgrade, Vol. 3, 105-108 (1989).

[4] J. O. Smith, "Efficient simulation of the reed-bore and bow-string mechanisms," In Proc. Int. Computer Music Conf., The Hague, 275-280 (1986).

[5] J. O. Smith, "Physical modeling synthesis update," Computer Music J. **20**(2), 44-56 (1996).

[6] G.R. Plitnik, and W.J. Strong, "Numerical method for calculating input impedances of the oboe," J. Acoust. Soc. Am. **65**(3), 816-825 (1979).

[7] R. Caussé, J. Kergomard, and X. Lurton, "Input impedance of brass musical instruments. Comparison between experiment and numerical models," J. Acoust. Soc. Am. **75**, 241-254 (1984).

[8] R. D. Ayers, L. J. Eliason, and D. Mahgerefteh, "The conical bore in musical acoustics," Am. J. of Physics **53**(6), 528-537 (1985).

[9] J. Agulló, A. Barjau, and J. Martínez, "Alternatives to the impulse response $h(t)$ to describe the acoustical behavior of conical ducts," J. Acoust. Soc. Am. **84**(5), 1606-1612 (1988).

[10] J. Martínez, and J. Agulló, "Conical bores. Part I: Reflection functions associated with discontinuities," J. Acoust. Soc. Am. **84**(5), 1613-1619 (1988).

[11] J.-D. Polack, "Time domain solution of Kirchhoff's Equation for sound propagation in viscothermal gases: a diffusion process," J. d'Acoustique **4**(1), 47-67 (1991).

[12] B. Gazengel, J. Gilbert, and N. Amir, "Time domain simulation of single reed wind instrument. From the measured input impedance to the synthesis signal. Where are the traps?," Acta Acustica **3**, 445-472 (1995).

[13] J. O. Smith, "Waveguide simulation of non-cylindrical acoustic tubes," In Proc. Int. Computer Music Conf., Montreal, 304-307 (1991).

[14] E. Ducasse, "Modélisation d'instruments de musique pour la synthèse sonore : application aux instruments à vent (Physical modeling synthesis of wind instruments)," In Colloque de Physique (Sup.) **52**(C2), Lyon, France, 837-840 (1990).

[15] V. Välimäki, T. I. Laakso, M. Karjalainen, and U. K. Laine, "A new computational model for the clarinet," In Proc. Int. Computer Music Conf., San Jose, California, (1992).

[16] M. van Walstijn, J. S. Cullen, and D. M. Campbell, "Modeling viscothermal wave propagation in wind instrument air columns," In Proc. Int. Symp. Musical Acoustics, Vol. **19**, Edimburgh, 413-418 (1997).

[17] M. van Walstijn, and J. O. Smith, "Use of truncated infinite impulse response (TIIR) filters in implementing efficient digital waveguide models of flared horns and piecewise conical bores with unstable one-pole filter elements," In Proc. Symp. Musical Acoustics, Leavenworth, Washington, 309-314 (1998).

[18] D.P. Berners, "Acoustics ans Signal Processing Techniques for Physical Modeling of Brass Instruments," PhD Thesis, Stanford University (1999).

[19] J. Martínez, J. Agulló, and S. Cardona, "Conical bores. Part II: Multiconvolution," J. Acoust. Soc. Am. **84**(5), 1620-1627 (1988).

[20] D. Matignon, "Représentation en variables d'état de modèles de guides d'ondes avec dérivation fractionnaire (State variables representation of waveguides including fractional derivation)," Thèse de l'Université Paris XI, Orsay, France, 1994.

[21] V. Välimäki, and M. Karjalainen, "Digital waveguide modeling of wind instrument bores constructed of truncated cones," In Proc. Int. Computer Music Conf., Aarhus, Denmark, 423-430 (1994).

[22] N. Amir, U. Shimony, and G. Rosenhouse, "A discrete model for tubular acoustic systems with varying cross section - the direct and inverse problems. Part 1: Theory," Acustica **81**, 450-462 (1995).

[23] G.P. Scavone, "An Acoustic Analysis of Single-Reed Woodwind Instruments with an Emphasis on Design and Performance Issues and Digital Waveguide Modeling Techniques," PhD Thesis, Stanford University (1997).

[24] T.I. Laakso, V. Välimäki, M. Karjalainen, and U.K. Laine, "Splitting the unit delay - tools for fractional delay filter design," IEEE Signal Proc. Mag. **13**(1), 30-60 (1996).

[25] S. Tassart, and P. Depalle, "Analytical approximations of fractional delays: Lagrange interpolators and allpass filters," In Proc. IEEE ICASSP 97, Munich, Germany, 455-458 (1997).

[26] A.G. Webster, "Acoustical impedance, and the theory of horns and of the phonograph," In Proc. Nat. Acad. Sci. (US), Vol. **5**, 275-282 (1919).

[27] V. Salmon, "Generalizes plane wave horn theory," J. Acoust. Soc. Am. **17**, 199-211 (1946).

[28] A.F. Stevenson, "Exact and approximate equations for wave propagation in acoustic horns," J. Appl. Phys. **22**, 1461-1463 (1951).

[29] A.H. Benade, and E.V. Jansson, "On plane and spherical waves in horns with nonuniform flare," Acustica **31**, 79-98 and 185-202 (1974).

[30] N.H. Fletcher, and T.D. Rossing, "The Physics of Musical Instruments (2nd Edition)," Springer-Verlag, New-York, 1998.

[31] A.H. Benade, "Equivalent circuits for conical waveguides," J. Acoust. Soc. Am. **83**(5), 1764-1769 (1988).

[32] C.J. Nederveen, "Acoustical Aspects of Woodwind Instruments (revised edition)," Northern Illinois University Press, DeKalb, Illinois 60115, 1998.

[33] J. Kergomard, J.-D. Polack, and J. Gilbert, "Vitesse de propagation d'une onde plane impulsionnelle dans un tuyau sonore (Propagation speed of an impulsional plane wave in a sound pipe)," J. d'Acoustique **4**, 467-483 (1991).

[34] A.M. Bruneau, M. Bruneau, Ph. Herzog, and J. Kergomard, "Boundary layer attenuation of higher order modes in waveguides," J. Sound Vib. **119**(1), 15-27 (1987).

[35] J.D. Polack, X. Meynial, J. Kergomard, C. Cosnard, and M. Bruneau, "Reflection function of a plane sound wave in a cylindrical tube," Revue Phys. Appl. **22**, 331-337 (1987).

[36] X. Meynial, "Systèmes micro-intervalles pour instruments à trous latéraux (Micro-intervals systems for wind instruments with tone holes)," Thèse de Docteur-Ingénieur, Université du Maine, Le Mans, France, 1987.

[37] J. Gilbert, J. Kergomard, and J.-D. Polack, "On the reflection functions associated with discontinuities in conical bores," J. Acoust. Soc. Am. **87**(4), 1773-1780 (1990).

[38] J. Agulló, A. Barjau, and J. Martínez, "On the time-domain description of conical bores," J. Acoust. Soc. Am. **91**(2), 1099-1105 (1992).

[39] L. Schwartz, "Théorie des distributions (Theory of Distributions) ," second edition, Hermann, Paris, France, 1966.

[40] W. H. Press, S. A. Teukolsky, W. T. Vetterling, and B. Flannery, "Integration of ordinary differential equations," In "Numerical Recipes in C. The Art of Scientific Computing. 2nd Edition," Chapter 16, 707-752 (Cambridge University Press, New-York, 1992)

[41] L. R. Rabiner, J. H. McClellan, and T. W. Parks, "FIR digital filter design techniques using weighted-Chebyshev approximation," *Proc. IEEE* **63**, 595-610 (1975).

[42] A. Antoniou, "New improved method for the design of weighted-Chebyshev, nonrecursive, digital filters," *IEEE Trans. Circuits Syst.* **30**, 740-750 (1983).

[43] J. W. Adams, "FIR digital filters with least-squares stopbands subject to peak-gain constraints," *IEEE Trans. Circuits Syst.* **38**(4), 376-388 (1991).

[44] C. S. Burrus, J. A. Barreto, and I. W. Selesnick, "Iterative reweighted design of FIR filters," *IEEE Trans. Signal Proc.* **42**(11), 2926-2936 (1994).

[45] R. A. Vargas, and C. S. Burrus, "Adaptive iterative reweighted least squares design of L_p FIR filters," *Proc. ICCASSP 99*, vol. 3, Signal Processing, Theory and Methods, 1129-1132 (1999).

[46] W.-S. Lu, and T.-B. Deng, "An improved weighted least-squares design for variable fractional delay FIR filters,"*IEEE Trans. Signal Proc.* **46**(8), 1035-1040 (1999).

[47] H. Levine, and J. Schwinger, "On the radiation of sound from an unflanged circular pipe," Physical Review **73**, 383-406 (1948).

[48] M. Abramowitz, and I. Stegun, I., "Handbook of Mathematical Functions," National Bureau of Standards Appl. Math. Series, #55, U.S. Govt. Printing Office, Washington, D.C., 1964.